
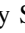






Tracing the Dynamical Mass in Galaxy Disks Using HI Velocity Dispersion and Its Implications for the Dark Matter Distribution in Galaxies

Mousumi Das¹ , Stacy S. McGaugh² , Roger Ianjamasimanana^{3,4} , James Schombert⁵ , and K. S. Dwarakanath⁶

¹Indian Institute of Astrophysics, Koramangala, Bangalore, Karnataka 560034, India; mousumi@iiaf.res.in, chandaniket@gmail.com

²Department of Astronomy, Case Western Reserve University, 10900 Euclid Avenue, Cleveland, OH 44106, USA

³Department of Physics and Electronics, Rhodes University, P.O. Box 94, Grahamstown 6140, South Africa

⁴South African Radio Astronomy Observatory, 2 Fir Street, Black River Park, Observatory 7925, Cape Town, South Africa

⁵Department of Physics, University of Oregon, 120 Willamette Hall, 1371 E 13th Avenue, Eugene, OR 97403461, USA

⁶Astronomy and Astrophysics, Raman Research Institute, C.V. Raman Avenue, 5th Cross Road, Sadashivanagar, Bengaluru, Karnataka 560080, India

Received 2019 August 28; revised 2019 December 2; accepted 2019 December 5; published 2020 January 20

Abstract

We present a method to derive the dynamical mass of face-on galaxy disks using their neutral hydrogen (HI) velocity dispersion (σ_{HI}). We have applied the method to nearby, gas-rich galaxies that have extended HI gas disks and have low inclinations. The galaxy sample includes four large disk galaxies, NGC 628, NGC 6496, NGC 3184, and NGC 4214, and three dwarf galaxies, DDO 46, DDO 63, and DDO 187. We have used archival HI data from The HI Nearby Galaxy Survey (THINGS) and the *LITTLE THINGS* survey to derive the HI gas distributions and *Spitzer* mid-infrared images to determine the stellar disk mass distributions. We examine the disk dynamical and baryonic mass ratios in the extreme outer disks where there is HI gas but no visible stellar disk. We find that for the large galaxies, the disk dynamical and HI gas mass surface densities are comparable in the outer disks. But in the smaller dwarf galaxies, for which the total HI gas mass dominates the baryonic mass, i.e., $M(\text{HI}) \geq M(\text{stars})$, the disk dynamical mass is much larger than the baryonic mass. For these galaxies, there must either be a very low-luminosity stellar disk which provides the vertical support for the HI gas disk or there is halo dark matter associated with their disks, which is possible if the halo has an oblate shape so that the inner part of the dark matter halo is concentrated around the disk. Our results are important for explaining the equilibrium of HI disks in the absence of stellar disks and is especially important for gas-rich, dwarf galaxies that appear to have significant dark matter masses associated with their disks.

Unified Astronomy Thesaurus concepts: Dwarf galaxies (416); Spiral galaxies (1560); HI line emission (690); Galaxy dark matter halos (1880); Galaxy disks (589); Dark matter distribution (356); Galaxy stellar disks (1594)

1. Introduction

Neutral hydrogen (HI) gas is one of the best tracers of the dynamical mass distributions in galaxies (de Blok et al. 2008; Oh et al. 2015). This is not only because of its cold, dissipational, nature but also because it is the most extended, visible component of disk galaxies with radii typically twice the size of the stellar disks (Swaters et al. 2002; Bigiel et al. 2010; Mishra et al. 2017). This is especially true for late-type galaxies and low-luminosity dwarfs, where the HI distribution is usually several times the radius of the visible disk (Swaters et al. 2002; Hunter et al. 2012). This makes HI an excellent tracer of galaxy rotation and the dynamical masses of galaxies (Bosma 1981; van Albada et al. 1985; Begeman 1989). Hence, it is also a good tracer of the dark matter distribution in galaxies (Katz et al. 2019).

The HI distribution and kinematics can also be used to constrain the halo density profiles of galaxies using their inner rotation curves (van den Bosch et al. 2000; Gentile et al. 2004; de Blok 2010). In recent times, this has become an important test of the cold dark matter (CDM) models of galaxy formation, which predict cuspy halo profiles rather than isothermal core profiles (cusp–core problem; Kuzio de Naray et al. 2008; de Blok 2010). The ideal galaxies for such studies are low surface brightness (LSB) dwarf galaxies that are dark matter dominated even in their inner disks (McGaugh & de Blok 1998). Studies of LSB galaxies have shown that they have the largest fraction of dark matter in our local Universe (de Blok &

McGaugh 1997) and their HI mass typically forms the major fraction of their baryonic mass (McGaugh et al. 2000).

Apart from measuring disk rotation, the HI disks in edge-on galaxies have been used to constrain the large-scale shape of dark matter halos (Olling 1995, 1996a; Banerjee et al. 2010; Peters et al. 2017). Warped HI disks have been used to investigate the alignment of the disk and halo angular momenta through modeling of the flared HI disks (Debattista & Sellwood 1999; Haan & Braun 2014). In all these studies, the vertical gravitational force binding the HI gas is assumed to be solely due to the stellar disk (Malhotra 1995; Patra et al. 2014). This assumption has also been used to model the vertical HI distribution and hence constrain the stellar disk height or vertical density profile (de Grijs & Peletier 1997).

In very general terms, the HI disk rotation is supported by the gravitational force of the galaxy and especially the dark matter halo. The vertical support of the HI disk is due to the stellar disk potential, which provides the gravity to bind the gas disk. Gravity tries to collapse the disk but is balanced by the velocity dispersion of the gas. Several mechanisms have been invoked to provide the energy input for the HI velocity dispersion, such as active galactic nucleus (AGN) activity or stellar winds that increase the HI velocity dispersion and turbulent gas pressure (Tamburro et al. 2009; Krumholz & Burkhardt 2016). However, the extended HI disks of galaxies such as LSB dwarfs and extreme late-type spirals are not generally associated with AGN activity nor do they have ongoing massive star formation (Das et al. 2007, 2019) and so

it is not clear what mechanism feeds the vertical dispersion of gas in such galaxies (Stilp et al. 2013).

A more puzzling problem is that galaxies with extended HI disks have hardly any visible disk mass in their outer regions. But a stellar disk is essential to provide the gravitational support for the vertical gas distribution, especially for HI-rich dwarf galaxies and LSB galaxies (Kreckel et al. 2011; Mishra et al. 2017), where even deep near-infrared (NIR) observations detect only very diffuse or low surface density stellar disks (Honey et al. 2016). For such galaxies, the stellar disk may not be massive enough to provide the vertical gravity for the extended HI disk and so the assumption that the HI disk is gravitationally supported by a stellar disk may not always hold. One of the ways to solve this problem is to include the presence of dark matter in galaxy disks so that it can help support the vertical equilibrium of the HI-dominated disks. The existence of disk dark matter was first postulated by Oort (1932) and has recently been studied by several authors as a component of the Galactic disk (Kalberla et al. 2007; Fan et al. 2013; Saburova & Zasov 2013; Kramer & Randall 2016). The disk dark matter could be part of an oblate halo or it could be mass that has settled within the disk as a result of mergers with satellite galaxies (Read et al. 2008).

In this study, we investigate the dynamical mass of the outer disks of galaxies using HI velocity dispersion σ_{HI} as a tracer of the local vertical disk potential. In the past few years, high-quality HI observations have made it possible to trace the radial distributions of σ_{HI} for a number of nearby galaxies (Ianjamasimanana et al. 2015, 2017; Mogotsi et al. 2016) as well as probe the cold and warm components of gas in nearby galaxies (Ianjamasimanana et al. 2012; Mogotsi et al. 2016). These studies show that large column densities of HI exist in regions where there is hardly any stellar disk mass, good examples being the gas-rich dwarfs DDO 63 and DDO 46 in the Local Irregulars That Trace Luminosity Extremes; The HI Nearby Galaxy Survey (LITTLE THINGS; Hunter et al. 2012).

In the following sections, we first derive an expression for the surface density of the disk dynamical mass assuming that the vertical gravitational support of the HI gas disk is solely due to the stellar and gas masses. We then use HI data from The HI Nearby Galaxy Survey (THINGS) and the *LITTLE THINGS* survey to determine the dynamical disk mass surface densities in seven nearby face-on disk galaxies and compare it with their baryonic mass surface densities using *Spitzer* Infrared Array Camera (IRAC) 3.6 μm images. Finally, we compare the dynamical and HI masses in the outer disks and discuss the implications of our results for understanding the dark matter distribution in galaxies.

2. The Disk Dynamical Mass

In this section, we derive an expression for the vertical equilibrium of a disk assuming only gravitational support from stars and gas. Our treatment is mainly applicable to the outer regions of gas-rich disk galaxies. We use HI as a tracer of the vertical potential so that the disk dynamical mass can be estimated using the HI velocity dispersion. There are two main conditions for applying this method. (i) There should be very little star formation and no nuclear activity in the regions where the dynamical mass is calculated as such activity will increase the turbulent gas velocity (v_{turb}) and the equations do not include v_{turb} . (ii) The disk should be close to face on, i.e., have low inclination. (iii) We ignore the molecular hydrogen (H_2)

gas mass. This is not a bad assumption for the outer regions of galaxy disks which contain little or no molecular gas (Dessauges-Zavadsky et al. 2014) or for LSB dwarf galaxies where CO is not detected (Das et al. 2006).

2.1. Derivation of the Disk Dynamical Mass Surface Density Σ_{dyn}

We start with the Jeans and Poisson equations for an axisymmetric system (Binney & Tremaine 1987). Assuming that the system is time independent and the velocities along the r , ϕ , z directions are independent, we have $-\rho_i \frac{d\Phi}{dz} = \frac{d[\rho_i \sigma_z^2]}{dz}$, where ρ_i represents the tracer density, and σ_z is the velocity dispersion in the vertical direction. Using the Poisson equation and assuming HI to be the tracer of the potential, we obtain the following equations:

$$\frac{1}{\rho_{\text{HI}}} \frac{d[\sigma_{z\text{HI}}^2 \rho_{\text{HI}}]}{dz} = -\frac{d\Phi}{dz}, \quad (1)$$

$$\frac{d^2\Phi}{dz^2} = 4\pi G[\rho_d + \rho_{\text{HI}}], \quad (2)$$

where ρ_d is the disk stellar mass density, ρ_{HI} is the HI gas density, and $\sigma_{z\text{HI}}$ is the HI disk velocity dispersion in the vertical or z -direction. Here we have assumed that the HI gas is a static, smooth atmosphere in equilibrium with the disk potential. The force in the vertical direction is given by

$$K_z(z) = -4\pi G \int_0^z [\rho_d + \rho_{\text{HI}}] dz. \quad (3)$$

If we assume that the stellar and gas disks have exponential mass distributions given by $\rho_d = \rho_e e^{-z/z_e}$ and $\rho_{\text{HI}} = \rho_{g0} e^{-z/z_{g0}}$ (van der Kruit 1988), where z is the distance from the $z = 0$ plane, then

$$\frac{1}{\rho_{\text{HI}}} \frac{d[\sigma_{z\text{HI}}^2 \rho_{\text{HI}}]}{dz} = -4\pi G z_e \rho_e (1 - e^{-z/z_e}) - 4\pi G z_{g0} \rho_{g0} (1 - e^{-z/z_{g0}}). \quad (4)$$

We have used an exponential form for the vertical mass distribution in the stellar disk and gas disk because it is the simplest form. Integrating both sides of the equation, from $z = 0$ to ∞ , we obtain

$$\int_0^\infty d[\sigma_{z\text{HI}}^2 \rho_{\text{HI}}] = -4\pi G z_e \rho_e \int_0^\infty (1 - e^{-z/z_e}) \rho_{\text{HI}} dz - 4\pi G z_{g0} \rho_{g0} \int_0^\infty (1 - e^{-z/z_{g0}}) \rho_{\text{HI}} dz. \quad (5)$$

The first integration on the right yields the term $-4\pi G z_e \rho_e \rho_{g0} \left(z_{g0} - \frac{z_{g0} z_e}{(z_{g0} + z_e)} \right)$, while the second gives $-2\pi G z_{g0}^2 \rho_{g0}^2$ (where $\int_0^\infty e^{-z/z_e} dz = z_e$ and $\int_0^\infty e^{-\frac{z}{z_{g0}}} dz = z_{g0}/2$). For the left-hand side, we can assume that the gas density vanishes at large z . Then, we obtain the following equation,

$$\frac{\sigma_{z\text{HI}}^2}{2\pi G z_{g0}} = 2 \frac{\rho_e z_e z_{g0}}{(z_e + z_{g0})} + \rho_{g0} z_{g0}. \quad (6)$$

Table 1
Galaxy Parameters

Galaxy Name	i (deg)	P.A (deg)	Distance (Mpc)	Spatial Scale	Galaxy Type	Magnitude Band	R_{25B} (arcsec)	$M(\text{H I})$ ($10^9 M_\odot$)	$M(\text{stars})$ ($10^9 M_\odot$)
NGC 628	7	20	7.3	35.4 pc/arcsec	SA(s)c, H II	9.76, B	360.0	5.2	15.0
NGC 6946	33	243	5.9	28.6 pc/arcsec	SAB(rs)cd;Sy2;H II	9.61, B	497.9	5.8	41.0
NGC 3184	16	179	11.1	53.8 pc/arcsec	SAB(rs)cd	10.3, B	255.0	3.9	23.4
NGC 4214	25.8	16	3.0	14.5 pc/arcsec	IAB(s)m	9.7, V	330.0	0.5	1.1
DDO 46	28	84	6.1	29.6 pc/arcsec	Im	13.32, V	66.0	0.21	0.03
DDO 63	0	0	3.9	18.9 pc/arcsec	IAB(s)m	13.22, V	120.0	0.17	0.04
DDO 187	39	37	2.2	10.7 pc/arcsec	ImIV-V	13.9, V	54.0	0.016	0.0083

Note. The inclination angles, position angles, and distance parameters have been listed from the *THINGS* survey (Walter et al. 2008) and the *LITTLE THINGS* survey (Hunter et al. 2012). The galaxy types, magnitudes, and sizes D_{25B} have been listed from NED. The H I and stellar masses were derived from the *THINGS* and *LITTLE THINGS* surveys using *ellint* as described in the text. Similarly, the stellar masses were derived using *Spitzer* 3.6 μm images.

The total disk surface density Σ_d including the stellar and gas components, is given by the relation

$$\Sigma_d = 2 \int_0^\infty (\rho_d + \rho_{\text{HI}}) dz = 2z_e \rho_e + 2z_{g0} \rho_{g0} \quad (7)$$

The z -component of the H I velocity dispersion $\sigma_{z\text{HI}}$ is hence related to the total stellar and gas mass disk surface densities, Σ_s and $\Sigma_{z\text{HI}}$, in the following way:

$$\frac{\sigma_{z\text{HI}}^2}{\pi G z_{g0}} = \frac{2z_{g0}}{(z_e + z_{g0})} \Sigma_s + \Sigma_{\text{HI}}. \quad (8)$$

This relation can also be written as

$$\frac{\sigma_{z\text{HI}}^2}{\pi G z_{g0}} = \Sigma_s + \Sigma_{\text{HI}} + \Sigma_s \frac{1 - \frac{z_e}{z_{g0}}}{1 + \frac{z_e}{z_{g0}}}. \quad (9)$$

Thus, the disk dynamical mass traced by $\sigma_{z\text{HI}}$ is composed of two parts. The first is the sum of the stellar and gas mass surface densities, whereas the second is a coupling term that is due to the difference in the scale heights of the stellar and gas disks. For example, if $z_e = z_{g0}$, then the third term in Equation (9) vanishes, and we have

$$\frac{\sigma_{z\text{HI}}^2}{\pi G z_e} = \Sigma_s + \Sigma_{\text{HI}}. \quad (10)$$

Until now, we have assumed that the vertical support is only due to the visible stellar disk and the H I gas mass. For the outer disks of galaxies where there is no visible stellar disk, $\Sigma_s \sim 0$. The left-hand side then represents the dynamical mass surface density of the disk and is given by

$$\Sigma_{\text{dyn}} = \frac{\sigma_{z\text{HI}}^2}{\pi G z_{g0}}. \quad (11)$$

The mean H I velocity dispersion in the z -direction $\sigma_{z\text{HI}}$ can be derived from the width of the H I velocity profiles of face-on galaxies (Petric & Rupen 2007; Ianjamasimanana et al. 2015). Then, using Equation (9), we can determine the dynamical mass in the disk (Σ_{dyn}). The value of Σ_{dyn} can be compared with the stellar and gas surface densities $\left(\Sigma_s + \Sigma_{\text{HI}} + \Sigma_s \frac{1 - \frac{z_e}{z_{g0}}}{1 + \frac{z_e}{z_{g0}}} \right)$, which can be determined from the NIR images and H I intensity maps.

This comparison is especially important for the outer disks of galaxies where there is no visible stellar disk supporting the H I disk. In these regions, the equilibrium is given simply by taking $\Sigma_s \approx 0$, so that we get $\Sigma_{\text{dyn}} = \Sigma_{\text{HI}}$. It must be noted that in

such cases when there is no visible stellar disk, the value of z_{g0} will correspond to the scale height of the dynamical mass component that provides the binding gravity for the H I gas disk. This is important for understanding the nature of the dynamical mass component, whether it is part of an oblate halo or whether it is dark matter within the disk as discussed in Section 5.

However, for disk regions where there is no visible stellar disk and $\Sigma_{\text{dyn}} > \Sigma_{\text{HI}}$, it means that the disk dynamical mass is larger than the detected baryonic mass of the disk. This could indicate the presence of a very low-luminosity, undetected stellar disk; alternatively, there could be halo dark matter associated with the disk in the form of an oblate inner halo or a thick disk. The mass surface density of the dark matter associated with the disk, Σ_{dm} , can be determined from the difference between the dynamical and H I disk, i.e.,

$$\Sigma_{dm} = \Sigma_{\text{dyn}} - \Sigma_{\text{HI}}. \quad (12)$$

In the following sections, we apply this method to the outer H I disks of four large galaxies that are close to face on and three dwarf galaxies that are also close to face on. Our main aim is to see if Σ_{dyn} is larger than Σ_{HI} in the outer regions of galaxy disks and if so, by how much.

2.2. Velocity Dispersion in a Near Face-on Disk

This method can be applied only to face-on galaxies that have an inclination angle (i) close to 0. This is to minimize the rotational velocity component along the line of sight so that the velocity gradient is smaller within the finite beam of the telescope. It allows a more reliable estimate of $\sigma_{z\text{HI}}$ from the width of the H I line profiles (van der Kruit & Shostak 1982). But such galaxies are hard to find, especially if high-resolution moment maps of the H I distribution are also essential. Hence, we have relaxed the criterion to include galaxies with $i < 40^\circ$ (Table 1). The value of $\sigma_{z\text{HI}}$ can then be approximately determined by averaging the values over concentric annuli in the disks. If we assume that $\sigma_{z\text{HI}}/\sigma_r = 0.5$ (Dehnen & Binney 1998), and using cylindrical coordinates (r, ϕ, z) for the disk, then from Das et al. (2019),

$$\sigma_{z\text{HI}}^2 = \frac{\sigma_{z\text{HI}}^2}{\cos^2 i + 4 \sin^2 i}, \quad (13)$$

where σ_{HI} is derived from the width of the H I profiles. The correction factor introduced in Equation (13) ranges in value from 1 (at 0°) to 0.45 (at 45°). It leads to a lower estimate of the

disk dynamical mass, so not using the correction would lead to higher dynamical mass estimates.

2.3. The Scale Height of the HI Gas Disk

Observations of edge-on disk galaxies show that the cool HI disk can have an FWHM of 260 pc in the central region of the disk but may flare out to an FWHM of 1.6 kpc in the extreme outer parts (Matthews & Wood 2003; Zschaechner & Rand 2015). In the HI plots of Matthews & Wood (2003), we find that to a first approximation, the HI disk thickness appears to be fairly uniform and has a value of $\approx \pm 30''$ or 0.75 kpc. The extended disks in these observations are similar to the HI-dominated outer disks of late-type galaxies and the diffuse disks of gas-rich dwarfs. Other observations of edge-on disk galaxies indicate that the HI disks have a $z_{1/2}(\text{HI})$ value of ≈ 0.5 kpc as shown in Figure 25 of O'Brien et al. (2010), unless there is a warping or flaring of the outer disk.

In our calculations, the $z_{1/2}(\text{HI})$ value represents the disk height that contains most of the HI mass. Hence, we have assumed the disk thickness corresponds to the density $0.1\rho_{g0}$, where $\rho_{\text{HI}} = \rho_{g0} e^{-z/z_{g0}}$. This height contains 90% of the HI surface density as shown below:

$$\Sigma_{\text{HI}} = 2 \int_0^{\ln 10} \rho_{g0} e^{-z/z_{g0}} dz = 0.9 \times 2\rho_{g0}z_{g0}. \quad (14)$$

Hence, the exponential scale height of the vertical HI gas distribution z_{g0} is related to the half z height $z_{1/2}$ by

$$z_{1/2} = \ln(10)z_{g0} = 2.3026z_{g0}. \quad (15)$$

An accurate estimate of Σ_{dyn} should include a radial variation of $z_{1/2}$ for both the stellar and HI disks as they both affect the values of Σ_{dyn} . But because this study is mainly aimed at comparing the Σ_{dyn} with the Σ_{HI} in the outer disks of galaxies, we will use constant dynamical disk width values of $z_{1/2} = 0.5$ kpc for the large disk galaxies (NGC 628, NGC 6946, NGC 3184, and NGC 4214). For the dwarf galaxies, because they have puffier stellar/HI disks (DDO 46, DDO 63, and DDO 187), we will use these two values of $z_{1/2} = 0.5$ and 1 kpc. The stellar disk thickness is relevant for only one galaxy (DDO 187) as discussed in Section 4. We will assume a similar relation as Equation (15) for the stellar exponential vertical scale length z_e .

3. Applying Our Method to Nearby Face-on Galaxies

3.1. Sample Selection

We have chosen our galaxies based on the following criteria:

(i) The HI gas should extend well beyond their star-forming stellar disks. This is because the expression in Equation (9) holds for HI disks in hydrostatic equilibrium, and this might not apply to regions where there are AGN outflows or massive star-forming regions which can increase the turbulent gas pressure and destroy the disk equilibrium. However, on average, over sections of the disk, the mechanical energy input from star formation may still produce a HI gas layer in dynamical equilibrium with the gravitational potential. So, our assumption is that whatever causes the HI velocity dispersion, the gas is largely in equilibrium from a dynamical standpoint.

(ii) The galaxies should be nearby so as to obtain several beamwidths across the disks and hence several values of the azimuthally averaged HI velocity dispersion.

(iii) The galaxies should have low inclinations in order to trace the vertical motion (z -direction). We have finally selected seven galaxies (Table 1) that have relatively high HI gas masses, are at distances 2–11 Mpc, and have inclinations less than 40° .

The first four galaxies, NGC 628, NGC 6946, NGC 3184, and NGC 4214, are large, late-type spirals that have HI to stellar disk mass ratios $M(\text{HI})/M(\text{star}) < 1$ (Table 1) and host star formation in their inner regions. But in all of them, the HI gas disk extends well beyond the R_{25} radius of the galaxy and the old stellar disk. They are all part of the *THINGS* survey (Walter et al. 2008). The galaxies NGC 628, NGC 6946, and NGC 3184 are grand-design spirals with moderate star formation rates (SFRs) of values 1–5, but NGC 4214 has a much lower SFR of 0.05 (Walter et al. 2008). The size, gas-rich nature, and SFR of NGC 4214 is more akin to that of late-type dwarf galaxies (Das et al. 2019) than large spirals. The galaxies NGC 628 and NGC 6946 also have compact H II regions in their outer disks (Ferguson et al. 1998; Lelièvre & Roy 2000), which is rare and often attributed to cold gas accretion from the intergalactic medium (IGM) which can trigger star formation (Thilker et al. 2007). Their outermost star-forming regions are associated with their inner spiral arms and can be traced into the outer disk using *GALEX* UV images (Gil de Paz et al. 2007).

Figure 1 shows an example of how the HI disk can extend well beyond the stellar disks of late-type galaxies such as NGC 628. The HI disk is about three times the size of the stellar disk. This is a well-known type I extended UV (XUV) galaxy (Thilker et al. 2007); such galaxies are characterized by UV emission from star formation along spiral arms in their extended disks. Most of the UV emission coincides with the stellar disk but faint trails of UV emission extend into the outer HI disk, following the disk spiral structure.

The remaining three galaxies, DDO 46, DDO 63, and DDO 187, are gas-rich dwarfs and are all part of the *LITTLE THINGS* survey (Hunter et al. 2012), which is a survey of nearby, gas-rich irregular/dwarf galaxies. All three galaxies have high HI to stellar disk mass ratios $M(\text{HI})/M(\text{star}) > 1$ (Table 1) but very low SFRs with values ranging from 0.001 to 0.005 (Hunter et al. 2012). Although they appear to be irregular in shape, they clearly have disks as indicated by their rotational to vertical velocity ratios $v_{\text{rot}}/\sigma_z > 1$ (Johnson et al. 2015). These classical low-luminosity dwarfs are dark matter dominated, and their rotation curves indicate that their dark matter halos have flat cores rather than cuspy profiles (Oh et al. 2015).

3.2. Archival Data

The HI maps of NGC 628, NGC 6946, NGC 3184, and NGC 4214 were obtained from *THINGS* and have a spectral resolution of either 2.6 km s^{-1} or 1.3 km s^{-1} and spatial resolution of $\sim 6''$ in the robust weighting scheme. This is important for obtaining a good HI surface density profile. For example, in NGC 628 (Table 1), the HI images have a spatial resolution of $\sim 6''$ or 212 pc assuming a distance of 7.3 Mpc. The HI velocity dispersions were derived by fitting a single Gaussian function to the HI emission profiles. For the dwarfs (DDO 46, DDO 63, DDO 187), the HI data were obtained from *LITTLE THINGS* (Hunter et al. 2012), which has a spectral resolution of either 2.6 km s^{-1} or 1.3 km s^{-1} and a spatial resolution of $\sim 6''$, which matches the resolution of *THINGS*. To derive the stellar masses, we used the mid-

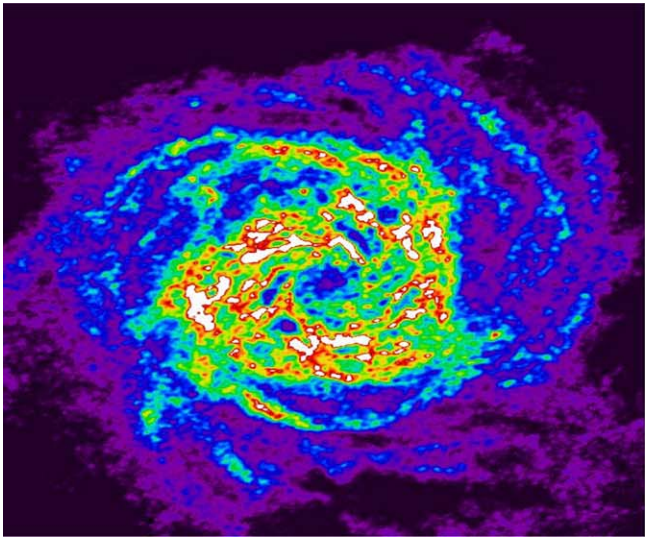


Figure 1. Images of NGC 628 at two different wavelengths, all on the same scale. The left panel is the moment 0 HI image from the *THINGS* survey, and the right-hand side panel is the IRAC 3.6 μm image. Note that the HI extends out to more than twice the stellar disk extent.

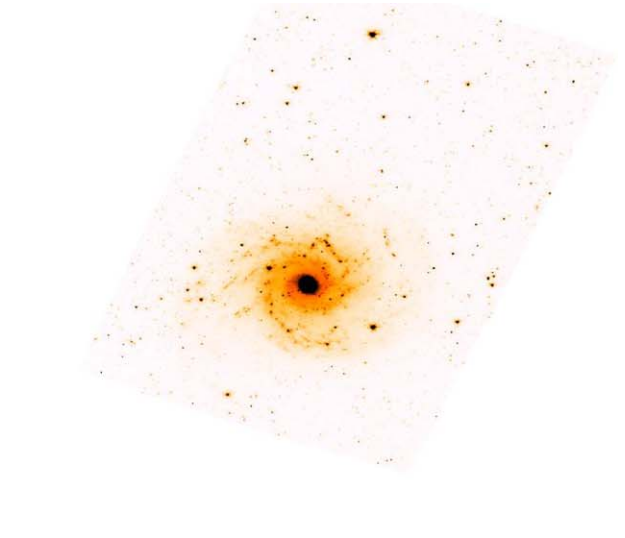
infrared (MIR, 3.6 μm) *Spitzer* IRAC images of the galaxies from the *Spitzer* Infrared Nearby Galaxies Survey (Kennicutt et al. 2003).

We have not included the molecular hydrogen gas (H_2) masses for the galaxies in this study mainly because we are interested in the dynamical masses of the outer disks of galaxies, where there is very little H_2 gas. These regions lie beyond the R_{25} radius, which is the radius at the optical 25 mag arcsec $^{-2}$ isophote. The molecular gas in the galaxies NGC 628, NGC 6946, NGC 3184, and NGC 4214 lie well within their R_{25} radii (Leroy et al. 2009). Molecular gas is not detected in DDO 63 (Leroy et al. 2009), DDO 46, or DDO 187 (Taylor et al. 1998).

3.3. The HI and Stellar Surface Densities

To determine the disk surface density for the HI disk, we used the MIRIAD task *ellint* to determine the mean and total fluxes within annuli of width equal to the mean beamwidth of the observations (Sault et al. 1995). The annuli were centered at the optical center of the galaxy, and we used a fixed inclination angle and position angle (Table 1), which are the same as those of *THINGS* (Walter et al. 2008). The HI mass was calculated using the relation $M(\text{HI}) = 1.4 \times 2.36 \times 10^5 D_{\text{Mpc}}^2 S_v$, where S_v is the flux in units of Jy km s $^{-1}$, and the multiplicative factor of 1.4 is the correction for including helium (Table 1).

To determine the stellar mass, we used a mass-to-light ratio of 0.5 (McGaugh & Schombert 2014; Table 1). Total luminosities were determined directly from archival IRAC images using the techniques outlined in McGaugh & Schombert (2014) from the 3.6 μm curve of growth. Note that the HI mass is an order of magnitude larger than the stellar mass for the dwarf galaxies but is comparable to the stellar mass in the large spiral galaxies (Table 1). The stellar 3.6 μm surface brightness at the outermost disk radii lies between 24 and 26 mag arcsec $^{-2}$ for the dwarf galaxies, but for the larger disk galaxies, it varies between 21 and 27 mag arcsec $^{-2}$. However, in all galaxies, the surface brightness profile has a decreasing trend in the outer disk (Figures 2 and 3) and the stellar disk mass surface density appears to be falling rapidly.



The figures in Section 4 show the surface mass density of HI and stars ($\Sigma(\text{HI})$, $\Sigma(s)$) for our sample. The stellar disk lies well within the R_{25} radii for all galaxies except for DDO 187. The HI gas disk is the most extended component, reaching out to twice the R_{25} radius for nearly all the galaxies except NGC 4214.

3.4. The HI Velocity Dispersion across the Disks

We followed the procedure outlined in Ianjamasimanana et al. (2012, 2017) while deriving the radial variations of the HI velocity dispersion across the HI disk of the galaxies. In summary, we line up individual velocity profiles to the same reference velocity and coadd them to get azimuthally averaged high signal-to-noise ratio (S/N) profiles. Note that only individual profiles with an S/N better than three times the rms noise level in a single channel map were coadded. We then fit the high-S/N stacked profiles with a single Gaussian function. The width of the fitted Gaussians represents the velocity dispersion of the bulk of the HI gas. As studied in detail in Ianjamasimanana et al. (2017; see also Ianjamasimanana et al. 2012 and Mogotsi et al. 2016), the stacking procedure outlined above effectively reduces the effects of noise in the derivation of the velocity dispersion. In addition, a Gaussian fit to the profile gives a more robust estimate of the velocity dispersion as opposed to the more straightforward moment map analysis. This is because moment map values are more prone to the effects of low-level uncleaned fluxes than single Gaussian fitting values unless a very careful clipping is applied. For a full discussion of this, we refer the reader to Ianjamasimanana et al. (2017). Note that in their papers, Ianjamasimanana et al. (2012, 2015) separate the HI profiles in terms of broad and narrow Gaussian components. Here, our choice of a single Gaussian fit is motivated by the fact that we are mainly interested in the outer disks of galaxies where the contributions of the narrow components to the global shapes of the azimuthally averaged velocity profiles are not important (for details see Ianjamasimanana et al. 2015). Thus, a separation into narrow and broad Gaussian components is not relevant for the purpose of this work. Figure 2 shows the radial variation of the velocity dispersion across the galaxy disks.

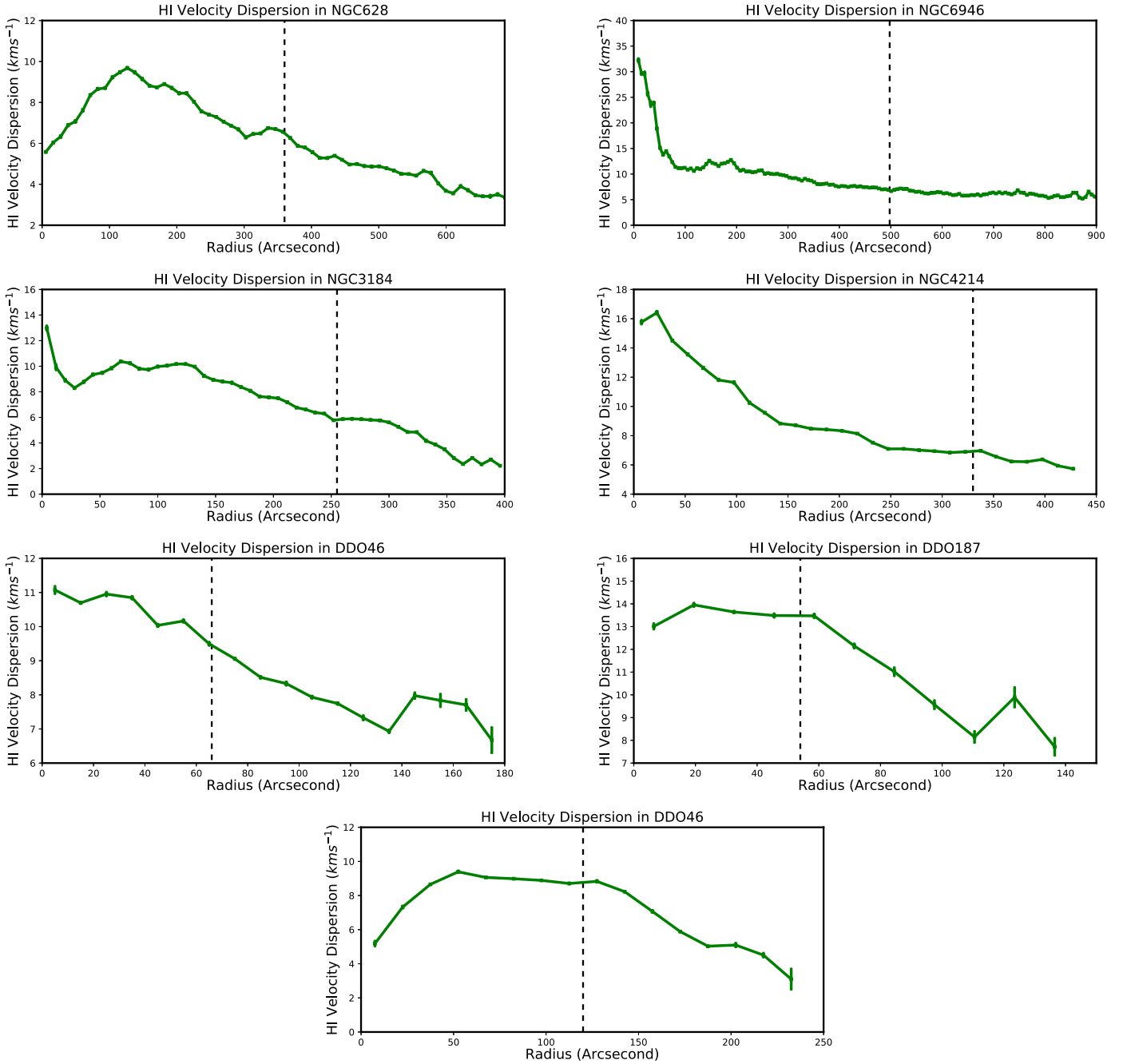


Figure 2. Radial variation of the HI velocity dispersion across the galaxy disks. The vertical dashed line marks the R_{25} radius for the galaxy (see Table 1).

Note that the large galaxies, and especially NGC 6946, clearly show nondeclining HI velocity dispersion in the outer parts of their disks.

The nearly face-on orientation of the galaxies in our sample means that the HI velocity dispersion closely traces the velocity in the z -direction (σ_{HI}). We use Equation (13) with the respective inclination angles (Table 1) to obtain $\sigma_{z\text{HI}}$. As reported in the literature, the velocity dispersions have a much shallower profile than the SFR density profiles even in the outer disks where star formation is absent or unimportant. This indicates that mechanisms other than star formation are also important to drive the line width of the HI.

4. Results

4.1. Dynamical and HI Masses of the Outer Disks

One of the main aims of this paper is to investigate what gravitationally binds the extended HI disks of galaxies in regions where there is no visible stellar disk. For example, Figures 3 and 4 show that the stellar disks traced by $3.6\mu\text{m}$ emission have smaller radii than the HI disks. Also, the stellar disks lie within the R_{25} radii for all galaxies except for DDO 187. Within the R_{25} radii of the large galaxies (Figure 1), the stellar mass surface density Σ_s is several magnitudes higher than Σ_{HI} . The gravity of the stellar disk maintains the vertical structure of the HI disk. The star formation within this region can give rise to turbulence in the gas, which can contribute to

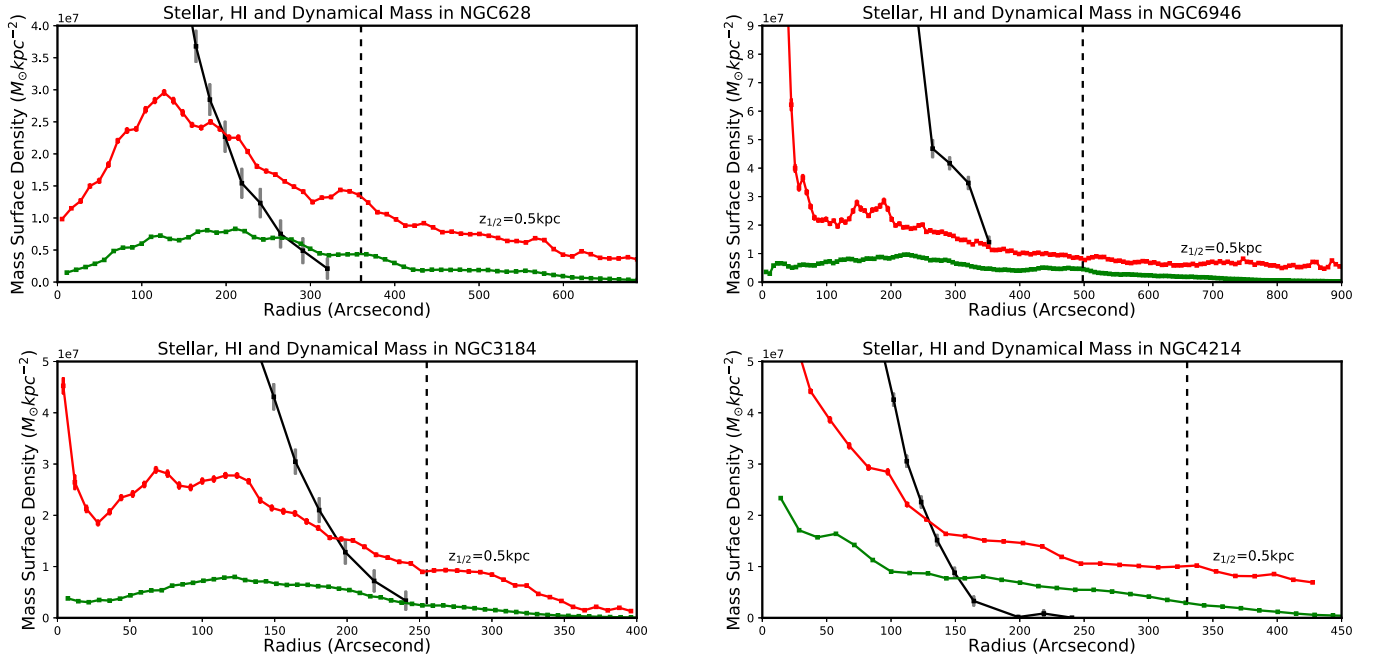


Figure 3. Surface mass density of stars $\Sigma(\text{stars})$ (black), H I $\Sigma(\text{H I})$ (green), and the dynamical mass derived from the H I velocity dispersion $\Sigma(\text{dyn})$ (red) for the large disk galaxies NGC 628, NGC 6946, NGC 3184, and NGC 4214. The disk half-width $z_{1/2}$ is assumed to be 0.5 kpc for all galaxies, and the dashed vertical line marks the R_{25} radius of the galaxy. Note that the dynamical mass density $\Sigma(\text{dyn})$ is comparable to $\Sigma(\text{H I})$ only in regions where there is very little stellar mass, which is usually in the extreme outer radii. All four galaxies have $M(\text{H I}) < M(\text{stars})$.

the gas pressure, which helps to balance the gravitational force of the disk.

But in the regions $R > R_{25}$, where the stellar disk surface density Σ_s is very low, there must be some other mass to gravitationally bind the H I disk because just the self-gravity of H I cannot maintain the vertical structure. We have applied our analytical results discussed in Section 2 to these regions, i.e., radii $R > R_{25}$, by assuming vertical equilibrium and applying Equation (11), i.e., $\Sigma_{\text{dyn}} = \sigma_{\text{zH I}}^2 / \pi G z_{g0}$. In Figure 3, we have compared Σ_{dyn} with $\Sigma_{\text{H I}}$ for the normal galaxies using the vertical disk height $z_{1/2} = 0.5$ kpc. Figure 4 shows the same for the dwarf galaxies but for two vertical disk scale heights, $z_{1/2} = 0.5$ and 1 kpc. Observations of edge-on galaxies suggest that $z_{1/2} = 0.5$ kpc is a good approximation for the vertical height of the H I layer in large disk galaxies (Zschaechner & Rand 2015). But dwarf galaxies have puffer H I disks, hence $z_{1/2} = 0.5$ kpc and 1 kpc are suitable values for this pilot study (Kamphuis et al. 2011). The assumption here is that the dynamical mass has a scale height similar to the H I vertical scale height. The Σ_{dyn} decreases for larger vertical disk heights, which is to be expected as the smaller $z_{1/2}$ values mean larger disk gravity and hence larger dynamical mass (Figure 4).

From Figure 3, it is clear that Σ_{dyn} as traced by the H I velocity dispersion is at least 1.5 to 2 times the value of $\Sigma_{\text{H I}}$ in the region $R > R_{25}$ for the galaxies NGC 628, NGC 3184, and NGC 4214. For NGC 6946, the difference between Σ_{dyn} and $\Sigma_{\text{H I}}$ is not very significant but because the disk is very extended, the total dynamical mass beyond R_{25} does become important. Table 2 shows the H I, stellar, and dynamical masses determined for the regions $R > R_{25}$. The upper radii for mass estimates are listed in column 6, and the R_{25} radii (in the B band) are given in Table 1. The upper radius is limited by the signal to noise of the H I velocity dispersion, which traces the dynamical mass. In the case of the gas-rich dwarf galaxies, M

(dyn) is much larger than $M(\text{H I})$ for nearly all radii (Figure 4) and especially for $R > R_{25}$. For radii $R < R_{25}$, the $M(\text{H I})$ is comparable to or larger than the stellar mass $M(\text{stars})$. This is not surprising as it is well known that the gas to stellar mass ratios are much higher for dwarfs, i.e., $M(\text{H I})/M(\text{stars}) \gg 1$ (Table 1). But for the outer radii ($R \gg R_{25}$), depending on the assumed vertical disk heights of the disks, the $M(\text{dyn})$ can vary from 2 to 14 times the value of $M(\text{H I})$. The most striking case is DDO 187, where $M(\text{dyn})$ is several times the value of $M(\text{H I})$ in the region $R > R_{25}$ for both $z_{1/2} = 0.5$ and 1 kpc (Table 2).

4.2. Comparison of the Dynamical to Baryonic Disk Masses for Radii $R > R_{25}$

To compare the dynamical and baryonic masses ($M(\text{H I}) + M(\text{stars})$) of our galaxies in the outer disk regions, we have summed over the surface densities Σ_{dyn} and $[\Sigma_{\text{H I}} + \Sigma_s]$ in the outer radii (Table 2). For all galaxies except DDO 187, we find that there is no stellar mass visible in the $3.6 \mu\text{m}$ NIR images at radii $R > R_{25}$. Hence, they have $M(\text{baryonic}) = M(\text{H I})$ for these regions. For the normal, large galaxies NGC 628, NGC 6946, NGC 3184, and NGC 4214, assuming a disk half-thickness or -height value of $z_{1/2} = 0.5$ kpc, the $M(\text{dyn})/M(\text{baryonic})$ varies between 4.4 and 5.2. But for the dwarf galaxies, because their stellar disks are more diffuse and maybe thicker, we have calculated $M(\text{dyn})/M(\text{baryonic})$ for $z_{1/2} = 0.5$ and 1 kpc (Table 2). It varies between 4.6 and 14.3 for $z_{1/2} = 0.5$, but varies between 2.3 and 7.2 for $z_{1/2} = 1$ kpc. As the disk thickness is increased, the difference between the dynamical and baryonic masses becomes smaller, which follows from the form of the expression for Σ_{dyn} (Equation (11)). $M(\text{dyn})/M(\text{baryonic})$ is largest for the gas-rich dwarf galaxy DDO 187. It is clear from Table 2 that for some of the dwarfs, the nonluminous mass associated with the disks is very significant and comparable to or more than the stellar disk mass of the galaxy (Table 1).

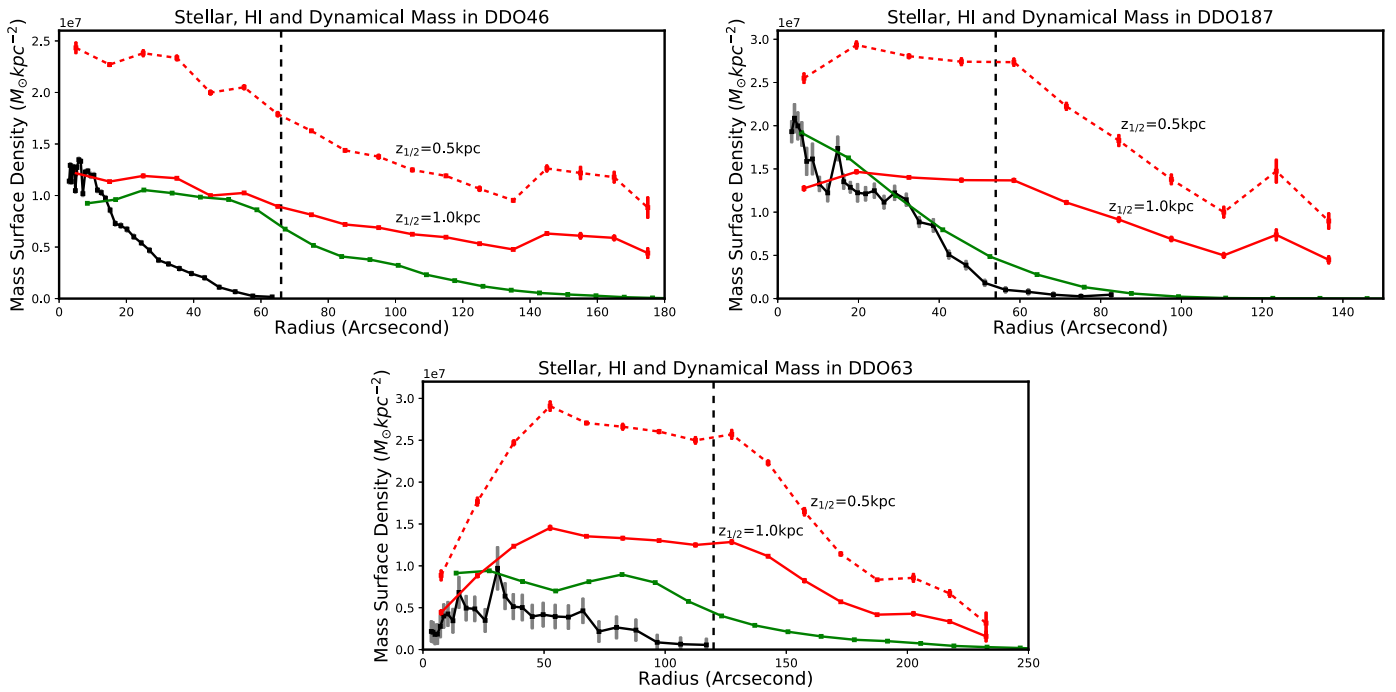


Figure 4. Surface mass density of stars Σ^* (black), H I $\Sigma(\text{H I})$ (green), and the dynamical mass derived from the H I velocity dispersion $\Sigma(\text{dyn})$ (red) for the gas-rich dwarf galaxies DDO 46, DDO 187, and DDO 63. The disk half-width $z_{1/2}$ is assumed to be 0.5 kpc and 1 kpc for all galaxies; the dashed vertical line marks the R_{25} radius. Note that the dynamical mass density $\Sigma(\text{dyn})$ is greater than $\Sigma(\text{H I})$ nearly over the entire galaxy disks.

An estimate of the nonluminous mass associated with the disks for the region $R > R_{25}$ is shown in the last column of Table 2. The values of $M_{\text{dyn}} - [M(\text{H I}) + M(\text{stars})]$ are of the order of $\sim 10^9 M_{\odot}$ for the larger galaxies (NGC 628, NGC 6946, NGC 3184) but around $\sim 10^7 - 10^8 M_{\odot}$ for the smaller/dwarf galaxies. In fact, for the dwarf galaxies, this mass is comparable to the stellar disk masses. The smaller galaxies are also the ones that are more gas rich and lower in luminosity. Hence, the outer disks of dwarf and low-luminosity galaxies maybe dark matter dominated as discussed in the next section. However, it must be noted that the mass in the disk region $R > R_{25}$ is in no way comparable to the total halo masses of the galaxies, which are typically 10–100 times the stellar masses in bright to low-luminosity galaxies. Our present sample consists of nearly face-on galaxies for which reliable rotation curves cannot be obtained and hence we cannot estimate the dark halo masses.

4.3. The Nondeclining Dynamical Masses of the Outer Disks

One of the surprising aspects of the H I velocity dispersion profiles of nearby galaxies is that it does not always fall rapidly to zero in the outer disks (Ianjamasimanana et al. 2015, 2017) (Figure 2), and hence the dynamical mass also does not decline (Figures 3 and 4). This is especially true in the case of the large galaxies NGC 628, NGC 6946, and NGC 4214 and the dwarfs DDO 46 and DDO 187, all of which clearly have nondeclining disk dynamical mass curves. This is somewhat similar to the rotation curves of galaxies where the nondeclining, flat rotation curves at large galactic radii indicate the presence of halo dark matter (Rubin et al. 1985; McGaugh et al. 2001; McGaugh 2014). Similarly, for the extended H I disks, the large differences between the disk dynamical masses and baryonic masses of face-on galaxies may indicate the presence of nonluminous disk mass extending out to radii well beyond the stellar disks. Deeper and more sensitive H I observations with upcoming telescopes such as the ngVLA or SKA will help

us probe these outer disk regions and put better constraints on the H I disk sizes of galaxies (Blyth et al. 2015).

5. Implications

One of the most important results of this study is that the baryonic mass surface density maybe lower than the dynamical mass surface density in the outer disks of galaxies, which implies that there is not enough baryonic mass (in the form of stars and H I gas) to bind the disk structure beyond R_{25} . This is clear from Table 2, which shows that $M_{\text{dyn}} / (M(\text{H I}) + M(\text{stars})) > 1$ in the region $R > R_{25}$. This could mean two things: (i) there is low-luminosity stellar mass in the outer disks which provides the gravity to maintain the vertical structure of the extended H I disks or (ii) there is dark matter associated with the disks.

For the first case, most of the low-luminosity mass has to be in the form of low-mass stars that are not detected in NIR observations. Deeper NIR observations could reveal more of this disk mass. However, the stellar mass profiles in Figures 3 and 4 indicate that the stellar mass distributions fall sharply near the R_{25} radius for all galaxies. So, a low-luminosity stellar disk providing the gravity for maintaining the disk in the region $R > R_{25}$ is unlikely.

If dark matter provides the gravitational force for binding the disk, it can have two possible origins. First of all, the dark matter could be the inner, denser part of the galaxy halo. In this scenario, the halo has a flattened or oblate shape, and so the inner halo is associated with the disk, which increases the mass surface density of the disk. The corresponding Σ_{dm} (Equation (12)) will increase the total mass surface density and support the vertical equilibrium of the H I disk. Oblate halo shapes have been investigated in earlier studies (Olling 1996a; Becaert & Combes 1997) using the H I velocity dispersion of nearby edge-on galaxies, but not with face-on galaxies as discussed in this paper. Olling (1996b) applied their method to

Table 2
Approximate Baryonic and Dynamical Masses in the Region $R > R_{25B}$

Galaxy Name	$M(\text{H I})$ (M_{\odot})	$M(\text{stars})$ (M_{\odot})	$z_{1/2}(\text{H I})$ (kpc)	$M(\text{dyn})$ (M_{\odot})	Relevant Radii	$\frac{M_{\text{dyn}}}{M(\text{H I}) + M(\text{stars})}$	$M_{\text{dyn}} - [M(\text{H I}) + M(\text{stars})]$ (M_{\odot})
NGC 628	2.05×10^9	...	0.5	9.11×10^9	$(1-1.9)R_{25B}$, (12.7–24.2) kpc	4.4	7.1×10^9
NGC 6946	2.05×10^9	...	0.5	9.62×10^9	$(1-1.8)R_{25B}$, (14.2–25.6) kpc	4.7	7.6×10^9
NGC 3184	8.79×10^8	...	0.5	4.56×10^9	$(1-1.6)R_{25B}$, (13.7–21.9) kpc	5.2	3.7×10^9
NGC 4214	9.16×10^7	...	0.5	4.33×10^8	$(1-1.3)R_{25B}$, (4.8–6.2) kpc	4.7	3.4×10^8
DDO 46	1.23×10^8	...	0.5	5.71×10^8	$(1-2.7)R_{25B}$, (2.0–5.3) kpc	4.6	4.5×10^8
		...	1.0	2.85×10^8		2.3	1.6×10^8
DDO 63	6.44×10^7	...	0.5	5.30×10^8	$(1-1.9)R_{25B}$, (2.3–4.3) kpc	8.2	4.7×10^8
		...	1.0	2.65×10^8		4.1	2.0×10^8
DDO 187	5.20×10^6	0.96×10^6	0.5	8.81×10^7	$(1-2.6)R_{25B}$, (0.58–1.5) kpc	14.3	8.2×10^7
			1.0	4.41×10^7		7.2	3.8×10^7

Note. The H I, stellar, and dynamical masses are derived for the regions $R > R_{25B}$. The lower and upper radii are listed in column 6, and the R_{25B} radii are given in Table 1.

NGC 4244 and their results suggest that the halo has an axis ratio of ~ 0.2 , which represents a very flat halo and could mean that the dark matter halo mass is associated with the extended H I disk. The method has also been applied to the Milky Way (Olling & Merrifield 2000), but the results suggest that the Milky Way halo is not oblate.

Flattened, nonspherical halo shapes may result from higher values of halo spin. Simulations suggest that low-luminosity galaxies, such as LSB galaxies, do have higher specific angular momentum and lower stellar disk surface densities (Kim & Lee 2013). In our study, we find that the low-luminosity dwarf galaxies have the largest $M_{\text{dyn}}/M(\text{baryon})$ ratios (Table 2) and the lowest disk surface densities. It is possible that this is due to an oblate halo shape, which can be due to a larger halo spin. A flattened dark matter distribution would also increase the midplane density of mass in the galaxy. If it has a similar scale height as the gas as assumed in this paper, it can be compared with the mass models derived from rotation curves (Carignan et al. 1990). We will be exploring this in a future study.

The second origin, the existence of disk dark matter, was first postulated by Oort (1932) who used it to explain the vertical equilibrium of old stars in the Galactic disk. It has also been invoked to explain the flaring of the Galactic gas disk (Kalberla et al. 2007) and has been included as a component of the Galactic disk in several studies (Fan et al. 2013; Saburova & Zasov 2013; Kramer & Randall 2016). The origin of disk dark matter has not been extensively explored but studies suggest that it could have formed as a result of mergers with satellite galaxies in Λ CDM simulations (Read et al. 2008). Other studies suggest that disk dark matter may be distinct from the halo dark matter and is clumpy in nature, because it has settled within the disk (Buckley & DiFranzo 2018).

Another important implication of our study is for star formation in the outer disks of galaxies. Star formation is triggered on global scales by processes such as galaxy interactions, mergers, spiral arms, and bar instabilities. Or it can be triggered by local events such as gas compression due to supernova shocks, stellar winds, and AGN outflows. But on smaller scales, it arises due to local disk instabilities that maybe sheared out into small, flocculent spiral arms. In the outer disks of isolated H I-dominated galaxies, there are no clear spiral arms or winds/outflows that can trigger star formation, and so local disk instabilities are the main cause for star formation in these regions. Early studies have shown that disk stability is

defined by a factor $Q = \kappa\sigma/\pi G\Sigma$ (commonly called the Toomre Q factor), where κ is the epicyclic frequency, σ_s is the stellar velocity dispersion, and Σ is the stellar mass surface density. If $Q < 1$, a disk is unstable to small perturbations (Safronov 1960; Toomre 1964). An expression for Q has also been derived for disks composed of gas and stars (Jog & Solomon 1984; Rafikov 2001). In all these cases, the disk becomes closer to instability as the mass surface density of baryons increases.

Many disk galaxies have compact regions of star formation in their outer disks (e.g., NGC 6946 and NGC 628) and are detected in H α emission (Ferguson et al. 1998; Barnes et al. 2012) or UV emission (Boissier et al. 2007; Gil de Paz et al. 2007; Thilker et al. 2007). However, a purely H I gas disk may not have the self-gravity to become unstable and form stars, and the Toomre Q factor due to H I alone is too high ($Q > 1$; Das et al. 2019). The presence of low-luminosity disk mass or halo dark matter associated with the disks can lower the Toomre Q factor, thus allowing local instabilities to form and leading to star formation (Krumholz & Burkhardt 2016). But not all galaxies may have enough disk mass in their outer regions to allow gravitational instabilities to develop. Hence, only galaxies with enough low-luminosity mass or dark matter in their outer disks can support star formation in these extreme environments.

Extended low-luminosity or dark matter disks are also important for the inside-out growth of galaxy disks driven by gas accreted via galaxy tidal interactions, major mergers, minor mergers (Heald et al. 2011; Marasco et al. 2019), or from the IGM from the filaments of the cosmic web (Kereš et al. 2005; Dekel et al. 2009; Kleiner et al. 2017; Noguchi 2018). Whatever the accretion process, star formation can proceed only if the disk mass surface density Σ is high enough to allow local or large-scale instabilities to develop. If the outer disk is already close to instability ($Q \sim 1$), then any increase in Σ due to external gas accretion can further lower the Q value and trigger local star formation. The importance of disk dark matter is that it can increase Σ in the outer extremities and aid the onset of star formation.

6. Conclusions

1. We have derived an analytical expression for estimating the dark matter in the disks of galaxies using the stellar and H I

gas distributions, and the mean HI velocity dispersion derived from fitting a single Gaussian function to azimuthally stacked HI profiles. Our method can be applied to face-on galaxies with extended HI disks.

2. We have applied our method to the extended HI disks of the large disk galaxies NGC 628, NGC 6946, NGC 3184, and NGC 4214, and the gas-rich dwarf galaxies DDO 46, DDO 63, DDO 187. We have used the distribution of HI velocity dispersion to derive the disk dynamical masses Σ_{dyn} and compared it with the disk baryonic masses in the regions $R > R_{25}$ using HI half-disk thickness values of 0.5 kpc for the large galaxies and half-disk thickness values of 0.5 kpc and 1 kpc for the smaller dwarf galaxies.

3. Our results show that for the large disk galaxies, $\Sigma_{\text{dyn}} > \Sigma_{\text{HI}}$ for $R > R_{25}$. But for the dwarf galaxies, $\Sigma_{\text{dyn}} > \Sigma_{\text{HI}}$ for nearly all radii and is the largest for DDO 187.

4. Our results mean that either there is a very low-luminosity stellar disk in the outer regions of the galaxies, or there is dark matter associated with the outer disks. The latter can occur if the halo is very oblate or if interactions with galaxies lead to the buildup of disk dark matter. The disk dark matter is important for supporting the HI gas layer in the extreme outer parts of galaxies where there appears to be no stellar disk.

5. The disk dark matter also has important implications for outer disk star formation as Σ_{dm} decreases the Toomre Q factor, and this can lead to the onset of local disk instabilities, and hence star formation. This is important for explaining the star formation in XUV disk galaxies and $\text{H}\alpha$ detected from star formation in the extreme outer disks of some local galaxies. It also suggests that gas accretion in galaxies can lead to outer disk star formation only when the Σ_{dm} is large enough to support local disk instabilities in the outer parts of galaxies.

The authors gratefully acknowledge IUSSTF grant JC-014/2017, which enabled the author M.D. to visit CWRU and develop the science presented in this paper. We also thank the anonymous referee for useful comments that improved the paper.

This research has made use of the NASA/IPAC Extragalactic Database (NED), which is operated by the Jet Propulsion Laboratory, California Institute of Technology, under contract with the National Aeronautics and Space Administration. This publication makes use of data products from the Spitzer Survey, which is a joint project of the University of Massachusetts and the Infrared Processing and Analysis Center/California Institute of Technology, funded by the National Aeronautics and Space Administration and the National Science Foundation. Funding for the SDSS and SDSS-II has been provided by the Alfred P. Sloan Foundation, the Participating Institutions, the National Science Foundation, the U.S. Department of Energy, the National Aeronautics and Space Administration, the Japanese Monbukagakusho, the Max Planck Society, and the Higher Education Funding Council for England. The SDSS Web Site is <http://www.sdss.org/>.





The SDSS is managed by the Astrophysical Research Consortium for the Participating Institutions. The Participating Institutions are the American Museum of Natural History, Astrophysical Institute Potsdam, University of Basel, University of Cambridge, Case Western Reserve University, University of Chicago, Drexel University, Fermilab, the Institute for Advanced Study, the Japan Participation Group, Johns Hopkins University, the Joint Institute for Nuclear

Astrophysics, the Kavli Institute for Particle Astrophysics and Cosmology, the Korean Scientist Group, the Chinese Academy of Sciences (LAMOST), Los Alamos National Laboratory, the Max-Planck-Institute for Astronomy (MPIA), the Max-Planck-Institute for Astrophysics (MPA), New Mexico State University, Ohio State University, University of Pittsburgh, University of Portsmouth, Princeton University, the United States Naval Observatory, and the University of Washington.

Facilities: Spitzer, VLA.

Software: MIRIAD, SAOIMAGE.

ORCID iDs

Mousumi Das  <https://orcid.org/0000-0001-8996-6474>
 Stacy S. McGaugh  <https://orcid.org/0000-0002-9762-0980>
 Roger Ianjamasimanana  <https://orcid.org/0000-0003-2476-3072>
 James Schombert  <https://orcid.org/0000-0003-2022-1911>

References

- Banerjee, A., Matthews, L. D., & Jog, C. J. 2010, *NewA*, **15**, 89
 Barnes, K. L., van Zee, L., Côté, S., & Schade, D. 2012, *ApJ*, **757**, 64
 Becquaert, J. F., & Combes, F. 1997, *A&A*, **325**, 41
 Begeman, K. G. 1989, *A&A*, **223**, 47
 Bigiel, F., Leroy, A., Walter, F., et al. 2010, *AJ*, **140**, 1194
 Binney, J., & Tremaine, S. 1987, *Galactic Dynamics* (Princeton, NJ: Princeton Univ. Press)
 Blyth, S., van der Hulst, T. M., Verheijen, M. A. W., et al. 2015, Exploring Neutral Hydrogen and Galaxy Evolution with the SKA in Proceedings of Advancing Astrophysics with the Square Kilometre Array (AASKA14) (Trieste: SISSA)
 Boissier, S., Gil de Paz, A., Boselli, A., et al. 2007, *ApJS*, **173**, 524
 Bosma, A. 1981, *AJ*, **86**, 1791
 Buckley, M. R., & DiFranzo, A. 2018, *PhRvL*, **120**, 051102
 Carignan, C., Charbonneau, P., Boulanger, F., & Viallefond, F. 1990, *A&A*, **234**, 43
 Das, M., Kantharia, N., Ramya, S., et al. 2007, *MNRAS*, **379**, 11
 Das, M., O’Neil, K., Vogel, S. N., & McGaugh, S. 2006, *ApJ*, **651**, 853
 Das, M., Sengupta, C., & Honey, M. 2019, *ApJ*, **871**, 197
 de Blok, W. J. G. 2010, *AdAst*, **2010**, 789293
 de Blok, W. J. G., & McGaugh, S. S. 1997, *MNRAS*, **290**, 533
 de Blok, W. J. G., Walter, F., Brinks, E., et al. 2008, *AJ*, **136**, 2648
 de Grijs, R., & Peletier, R. F. 1997, *A&A*, **320**, L21
 Debattista, V. P., & Sellwood, J. A. 1999, *ApJL*, **513**, L107
 Dehnen, W., & Binney, J. J. 1998, *MNRAS*, **298**, 387
 Dekel, A., Birnboim, Y., Engel, G., et al. 2009, *Natur*, **457**, 451
 Dessauges-Zavadsky, M., Verdugo, C., Combes, F., & Pfenniger, D. 2014, *A&A*, **566**, A147
 Fan, J., Katz, A., Randall, L., & Reece, M. 2013, *PDU*, **2**, 139
 Ferguson, A. M. N., Wyse, R. F. G., Gallagher, J. S., & Hunter, D. A. 1998, *ApJL*, **506**, L19
 Gentile, G., Salucci, P., Klein, U., Vergani, D., & Kalberla, P. 2004, *MNRAS*, **351**, 903
 Gil de Paz, A., Boissier, S., Madore, B. F., et al. 2007, *ApJS*, **173**, 185
 Haan, S., & Braun, R. 2014, *MNRAS*, **440**, L21
 Heald, G., Józsa, G., Serra, P., et al. 2011, *A&A*, **526**, A118
 Honey, M., Das, M., Ninan, J. P., & Manoj, P. 2016, *MNRAS*, **462**, 2099
 Hunter, D. A., Ficut-Vicas, D., Ashley, T., et al. 2012, *AJ*, **144**, 134
 Ianjamasimanana, R., de Blok, W. J. G., & Heald, G. H. 2017, *AJ*, **153**, 213
 Ianjamasimanana, R., de Blok, W. J. G., Walter, F., et al. 2015, *AJ*, **150**, 47
 Ianjamasimanana, R., de Blok, W. J. G., Walter, F., & Heald, G. H. 2012, *AJ*, **144**, 96
 Jog, C. J., & Solomon, P. M. 1984, *ApJ*, **276**, 114
 Johnson, M. C., Hunter, D., Wood, S., et al. 2015, *AJ*, **149**, 196
 Kalberla, P. M. W., Dedes, L., Kerp, J., & Haud, U. 2007, *A&A*, **469**, 511
 Kamphuis, P., Peletier, R. F., van der Kruit, P. C., & Heald, G. H. 2011, *MNRAS*, **414**, 3444
 Katz, H., Desmond, H., McGaugh, S., & Lelli, F. 2019, *MNRAS*, **483**, L98
 Kennicutt, R. C., Jr., Armus, L., Bendo, G., et al. 2003, *PASP*, **115**, 928
 Kereš, D., Katz, N., Weinberg, D. H., & Davé, R. 2005, *MNRAS*, **363**, 2
 Kim, J.-h., & Lee, J. 2013, *MNRAS*, **432**, 1701

- Kleiner, D., Pimblett, K. A., Jones, D. H., Koribalski, B. S., & Serra, P. 2017, *MNRAS*, **466**, 4692
- Kramer, E. D., & Randall, L. 2016, *ApJ*, **829**, 126
- Kreckel, K., Peebles, P. J. E., van Gorkom, J. H., van de Weygaert, R., & van der Hulst, J. M. 2011, *AJ*, **141**, 204
- Krumholz, M. R., & Burkhardt, B. 2016, *MNRAS*, **458**, 1671
- Kuzio de Naray, R., McGaugh, S. S., & de Blok, W. J. G. 2008, *ApJ*, **676**, 920
- Lelièvre, M., & Roy, J.-R. 2000, *AJ*, **120**, 1306
- Leroy, A. K., Walter, F., Bigiel, F., et al. 2009, *AJ*, **137**, 4670
- Malhotra, S. 1995, *ApJ*, **448**, 138
- Marasco, A., Fraternali, F., Heald, G., et al. 2019, *A&A*, **631**, A50
- Matthews, L. D., & Wood, K. 2003, *ApJ*, **593**, 721
- McGaugh, S. 2014, *Galax*, **2**, 601
- McGaugh, S. S., & de Blok, W. J. G. 1998, *ApJ*, **499**, 41
- McGaugh, S. S., Rubin, V. C., & de Blok, W. J. G. 2001, *AJ*, **122**, 2381
- McGaugh, S. S., & Schombert, J. M. 2014, *AJ*, **148**, 77
- McGaugh, S. S., Schombert, J. M., Bothun, G. D., & de Blok, W. J. G. 2000, *ApJL*, **533**, L99
- Mishra, A., Kantharia, N. G., Das, M., Omar, A., & Srivastava, D. C. 2017, *MNRAS*, **464**, 2741
- Mogotsi, K. M., de Blok, W. J. G., Caldú-Primo, A., et al. 2016, *AJ*, **151**, 15
- Noguchi, M. 2018, *ApJ*, **853**, 67
- O'Brien, J. C., Freeman, K. C., & van der Kruit, P. C. 2010, *A&A*, **515**, A61
- Oh, S.-H., Hunter, D. A., Brinks, E., et al. 2015, *AJ*, **149**, 180
- Olling, R. P. 1995, *AJ*, **110**, 591
- Olling, R. P. 1996a, *AJ*, **112**, 481
- Olling, R. P. 1996b, *AJ*, **112**, 457
- Olling, R. P., & Merrifield, M. R. 2000, *MNRAS*, **311**, 361
- Oort, J. H. 1932, *BAN*, **6**, 249
- Patra, N. N., Banerjee, A., Chengalur, J. N., & Begum, A. 2014, *MNRAS*, **445**, 1424
- Peters, S. P. C., van der Kruit, P. C., Allen, R. J., & Freeman, K. C. 2017, *MNRAS*, **464**, 65
- Petric, A. O., & Rupen, M. P. 2007, *AJ*, **134**, 1952
- Rafikov, R. R. 2001, *MNRAS*, **323**, 445
- Read, J. I., Lake, G., Agertz, O., & Debattista, V. P. 2008, *MNRAS*, **389**, 1041
- Rubin, V. C., Burstein, D., Ford, W. K., Jr., & Thonnard, N. 1985, *ApJ*, **289**, 81
- Saburova, A. S., & Zasov, A. V. 2013, *AN*, **334**, 785
- Safronov, V. S. 1960, *AnAp*, **23**, 979
- Sault, R. J., Teuben, P. J., & Wright, M. C. H. 1995, in ASP Conf. Ser. 77, *Astronomical Data Analysis Software and Systems IV*, ed. R. A. Shaw, H. E. Payne, & J. J. E. Hayes (San Francisco, CA: ASP), 433
- Stilp, A. M., Dalcanton, J. J., Skillman, E., et al. 2013, *ApJ*, **773**, 88
- Swaters, R. A., van Albada, T. S., van der Hulst, J. M., & Sancisi, R. 2002, *A&A*, **390**, 829
- Tamburro, D., Rix, H.-W., Leroy, A. K., et al. 2009, *AJ*, **137**, 4424
- Taylor, C. L., Kobulnicky, H. A., & Skillman, E. D. 1998, *AJ*, **116**, 2746
- Thilker, D. A., Bianchi, L., Meurer, G., et al. 2007, *ApJS*, **173**, 538
- Toomre, A. 1964, *ApJ*, **139**, 1217
- van Albada, T. S., Bahcall, J. N., Begeman, K., & Sancisi, R. 1985, *ApJ*, **295**, 305
- van den Bosch, F. C., Robertson, B. E., Dalcanton, J. J., & de Blok, W. J. G. 2000, *AJ*, **119**, 1579
- van der Kruit, P. C. 1988, *A&A*, **192**, 117
- van der Kruit, P. C., & Shostak, G. S. 1982, *A&A*, **105**, 351
- Walter, F., Brinks, E., de Blok, W. J. G., et al. 2008, *AJ*, **136**, 2563
- Zschaechner, L. K., & Rand, R. J. 2015, *ApJ*, **808**, 153